Science
AAAS

Spatial organization of cytokinesis signaling reconstituted in a cell-free system

Phuong A. Nguyen *et al.*

Science **346**, 244 (2014);
DOI: 10.1126/science.1256773

ability to quantify progress toward targets (*23*). The benefits of maintaining biodiversity are well known (*24*). Our results provide a baseline against which to measure progress toward this objective in 2020 and suggest that efforts need to be redoubled to positively affect trajectories of change and enable global biodiversity goals to be met by the end of the current decade.

REFERENCES AND NOTES

1. United Nations, *Convention on Biological Diversity* (Rio de Janeiro, Brazil, 1992).
2. Secretariat of the Convention on Biological Diversity (SCBD), "Handbook of the Convention on Biological Diversity" (Earthscan, London, 2003).
3. B. Worm *et al*., *Science* **325**, 578–585 (2009).
4. S. H. M. Butchart *et al*., *Science* **328**, 1164–1168 (2010).
5. SCBD, "Global Biodiversity Outlook 3" (Montreal, 2010).
6. UNEP, CBD, "UNEP/CBD/COP/DEC/X/2 2010" (2010).
7. T. H. Sparks *et al*., *Oryx* **45**, 411–419 (2011).
8. See supplementary materials on *Science* Online.
9. UNEP, CBD, UNEP/CBD/COP/DEC/XI/3 2012 (2012).
10. J. Durbin, S. J. Koopman, *Time Series Analysis by State Space Methods* (Oxford Univ. Press, Oxford, 2001).
11. K. P. Burnham, D. R. Anderson, *Model Selection and Multi-Model Inference: A Practical Information-Theoretic Approach* (Springer, New York, ed. 2, 2002).
12. CBD, Programme of Work on Protected Areas (PoWPA), https://www.cbd.int/protected/implementation/actionplans/ (2013).
13. D. P. McCarthy *et al*., *Science* **338**, 946–949 (2012).
14. Furthermore, the ability of statistical models to react to recent changes in indicator trends will vary depending on, among other things, the length of the time series, the noise in the data, and the magnitude of departure from the previous trend.
15. J. M. Bullock, J. Aronson, A. C. Newton, R. F. Pywell, J. M. Rey-Benayas, *Trends Ecol. Evol.* **26**, 541–549 (2011).
16. J. P. Metzger *et al*., *Biol. Conserv.* **142**, 1166–1177 (2009).
17. M. Di Marco *et al*., *Conserv. Biol.* **28**, 1109–1118 (2014).
18. D. Nepstad *et al*., *Science* **344**, 1118–1123 (2014).
19. M. Walpole *et al*., *Science* **325**, 1503–1504 (2009).
20. H. M. Pereira, L. M. Navarro, I. S. Martins, *Annu. Rev. Environ. Resour.* **37**, 25–50 (2012).
21. It is also possible that the response, pressure, and state indicator framework is not tracking factors that are causally linked (*7*); use of this framework does not imply joined-up indicators.
22. M. Hoffmann *et al*., *Science* **330**, 1503–1509 (2010).
23. S. L. Pimm *et al*., *Science* **344**, 1246752 (2014).
24. B. J. Cardinale *et al*., *Nature* **486**, 59–67 (2012).

ACKNOWLEDGMENTS

We thank I. Arto, A. H.W. Beusen, C. Brown, L. Coad, L. Collette, R. de Groot, F. Essl, J. Geldmann, P. Genovesi, M. Harfoot, M. Hockings, I. Hoffmann, M. Hoffman, L. Joppa, D. Juffe-Bignoli, N. Kingston, F. Krausmann, V. Lam, B. MacSharry, M. McGeoch, L. McRae, H. Meng, B. O'Connor, D. Pritchard, W. Rabitsch, B. Russell, C. Smith, S. Stewart, P. Stoett, M van Oorschot, H. Visser, M. Wackernagel, A. Watkins, M. Wieczorek, B. Worm, and M. Zemp. A.G. acknowledges Global Footprint Network's Research team and MAVA Fondation pour la Nature. D.B. acknowledges support from NSERC Discovery grant to W.C. Leggett & K. T. Franmk. V.C. acknowledges support from the Natural Sciences and Engineering Research Council of Canada. W.C. acknowledges support from NF-UBC Nereus Program. S.R.J.H. acknowledges support from the National Science Foundation (DEB–1115025) and DIVERSITAS. S.C.B.D. and UNEP-WCMC acknowledge funding support from Canada, the European Union, Germany, Japan, Netherlands, the Republic of Korea, Switzerland, and the UK. All scripts and data used to conduct analyses are available at https://github.com/derekt/Aichi-2020-analysis.

SUPPLEMENTARY MATERIALS

www.sciencemag.org/content/346/6206/241/suppl/DC1
Materials and Methods
Supplementary Text
Figs. S1 to S55
Tables S1 to S8
References (*25*–*129*)

16 June 2014; accepted 15 September 2014
Published online 2 October 2014;
10.1126/science.1257484

CELL-FREE ASSAYS

Spatial organization of cytokinesis signaling reconstituted in a cell-free system

Phuong A. Nguyen,[1,2]* Aaron C. Groen,[1,2]* Martin Loose,[1] Keisuke Ishihara,[1,2] Martin Wühr,[1] Christine M. Field,[1,2]†‡ Timothy J. Mitchison[1,2]†

During animal cell division, the cleavage furrow is positioned by microtubules that signal to the actin cortex at the cell midplane. We developed a cell-free system to recapitulate cytokinesis signaling using cytoplasmic extract from *Xenopus* eggs. Microtubules grew out as asters from artificial centrosomes and met to organize antiparallel overlap zones. These zones blocked the interpenetration of neighboring asters and recruited cytokinesis midzone proteins, including the chromosomal passenger complex (CPC) and centralspindlin. The CPC was transported to overlap zones, which required two motor proteins, Kif4A and a Kif20A paralog. Using supported lipid bilayers to mimic the plasma membrane, we observed the recruitment of cleavage furrow markers, including an active RhoA reporter, at microtubule overlaps. This system opens further approaches to understanding the biophysics of cytokinesis signaling.

Actomyosin-based cleavage furrows in animal cells are positioned by signals emanating from microtubule assemblies formed shortly after anaphase onset (*1*). In typical somatic cells, the signaling complexes centralspindlin and the chromosomal passenger complex (CPC) accumulate at the center of the midzone (or central spindle), which forms in the space previously occupied by the mitotic spindle (*2*). It is unclear how the microtubules that position furrows are organized in much larger egg cells and how they signal to the cortex. We addressed these questions by developing a cell-free system to reconstitute the spatial signaling that is characteristic of cytokinesis in a large egg cell.

To reconstitute cytokinesis events, undiluted egg cytoplasm with intact actin (*3*), containing fluorescent probes and Aurora kinase A (AurkA)–based artificial centrosome beads (*4*), was treated with Ca^{2+} to mimic fertilization and immediately spread between two coverslips for imaging (fig. S1A). As the cell cycle progressed from metaphase to interphase (*5*), large microtubule asters grew out rapidly from each AurkA bead. Where the expanding edges of two neighboring asters met, antiparallel microtubule bundles formed in a boundary zone that we term the aster-aster interaction zone (AAIZ) (Fig. 1, A to C, fig. S1, and movie S1). In somatic cells, the CPC and centralspindlin complexes are recruited to the midplane in anaphase, where they specify the division plane by activating the small GTPase RhoA (*2*). We imaged endogenous complexes by adding labeled antibodies, and for the CPC we confirmed localization with a green fluorescent protein (GFP)–tagged DasraA subunit (*5*). CPC and the Kif23 subunit of centralspindlin were recruited to the AAIZ in a 5- to 15-μm-wide line bisecting the line between two AurkA beads (Fig. 1, B and C, and fig. S1). The AAIZ was wider than a somatic cell midzone and was hundreds of microns long. To evaluate its physiological relevance, we imaged the same proteins in *Xenopus* zygotes fixed between mitosis and cytokinesis, which takes place at interphase in early embryonic cells (Fig. 1D) (*6*). The morphology of the midplane in zygotes, as defined by microtubule morphology and CPC/centralspindlin localization, was strikingly similar to that of the AAIZ in extracts (Fig. 1, A to C).

To measure microtubule orientation at the AAIZ we tracked GFP-tagged end-binding protein 1 (EB1), which binds to growing microtubule plus ends (Fig. 1E, fig. S2, and movie S2) (*7*). Microtubules grew outward radially within each aster. At the AAIZ, EB1 comets from both directions entered antiparallel bundles, where they usually disappeared (Fig. 1E). We quantified the degree of interpenetration by categorizing EB1 comets based on their direction (fig. S3) (*5*). The AAIZ was characterized by a sharp change in directionality over ~20 μm, indicating a localized block to interpenetration between the asters (Fig. 1F).

Kinase activity of the Aurora kinase B (AurkB) subunit of the CPC is required to establish midzone morphology and for furrow ingression (*8*). We confirmed this in *Xenopus* eggs (fig. S4) (*5*). AurkB inhibition blocked recruitment of the CPC in our cell-free system (Fig. 1E) and caused much deeper interpenetration of microtubules (Fig. 1, E and F, and movie S3). Thus, AurkB activity was required to create a sharp boundary between asters.

CPC is proposed to be transported to the center of midzones along microtubules by a kinesin molecular motor (*9*), but transport has not been observed directly. Five plus-end–directed kinesins involved in cell division are candidates for CPC transport (*10*): Kif4A, Kif10 (also called CenpE),

[1]Department of Systems Biology, Harvard Medical School, Boston, MA 02115, USA. [2]Marine Biological Laboratory, Woods Hole, MA 02543, USA.
*These authors contributed equally to this work. †These authors contributed equally to this work. ‡Corresponding author. E-mail: Christine_Field@hms.harvard.edu

Kif11 (Eg5), Kif20A (Mklp2/Rabkinesin-6), and Kif23 (Mklp1, a subunit of centralspindlin). *Xenopus* eggs also contain an unusual kinesin 41% identical to Kif20A by sequence (*11*). This is likely to be an embryo-specific paralog, and we propose the name KIF20A embryonic, abbreviated KIF20AE. Small-molecule inhibition of Kif10 and Kif11, and depletion of somatic Kif20A and Kif23, had no effect on antiparallel microtubule bundling in the AAIZ or on CPC localization (Fig. 2, A and B, and figs. S5 and S6). Depletion of Kif4A did not block CPC accumulation or the assembly of antiparallel bundles, but increased the width of the CPC-positive zone; adding back recombinant Kif4A rescued this phenotype (Fig. 2A and fig. S6). Depletion of Kif20AE completely blocked CPC accumulation and disorganized the AAIZ (Fig. 2A). Thus, Kif20AE is absolutely required for CPC recruitment in eggs, presumably mirroring the Kif20A requirement in somatic cells (*9*), and Kif4A plays some role in focusing it.

Microtubule bundles in the AAIZ localized Kif20AE (Fig. 2C), Kif4A (Fig. 2D), and an embryonic paralog of PRC1 (PRC1E, an antiparallel microtubule crosslinker; fig. S1D), all of which have been shown to bind the CPC in pull-down experiments (*9*, *12*–*14*). Time-lapse imaging showed that CPC clusters moved to the center of the overlap zone at a rate of 10 to 25 μm/min, slowing as they reached the center (Fig. 2, E and F, fig. S7, and movie S4). Tubulin speckle imaging showed sliding of microtubules away from the overlap center at <5 μm/min (fig. S8 and movies S6 to S8). Thus, the observed CPC movement represents transport toward plus ends. The maximal transport rate was close to that of Kif4A in an isolated aster that was not part of an AAIZ (Fig. 2F, green line, and fig. S9) (*5*). Kif4A depletion blocked CPC movement, and addback of recombinant Kif4A rescued it (Fig. 2, E and F, fig. S10, and movie S5). Live imaging showed partial colocalization of CPC and Kif4A movement (fig. S11). Thus, the CPC is targeted to the AAIZ and transported to a narrow band by the combined action of Kif20AE and Kif4A. Transport probably slows as CPC engages binding sites in the AAIZ (*5*).

To test whether AAIZs in the cell-free system can signal to the cortex, we prepared supported lipid bilayers on glass coverslips, using lipids characteristic of the inner leaflet of animal cell plasma membranes, including phosphatidylinositol (PI) and phosphatidylinositol 4,5-bisphosphate [$PI(4,5)P_2$] (*5*, *15*). Protein recruitment was imaged

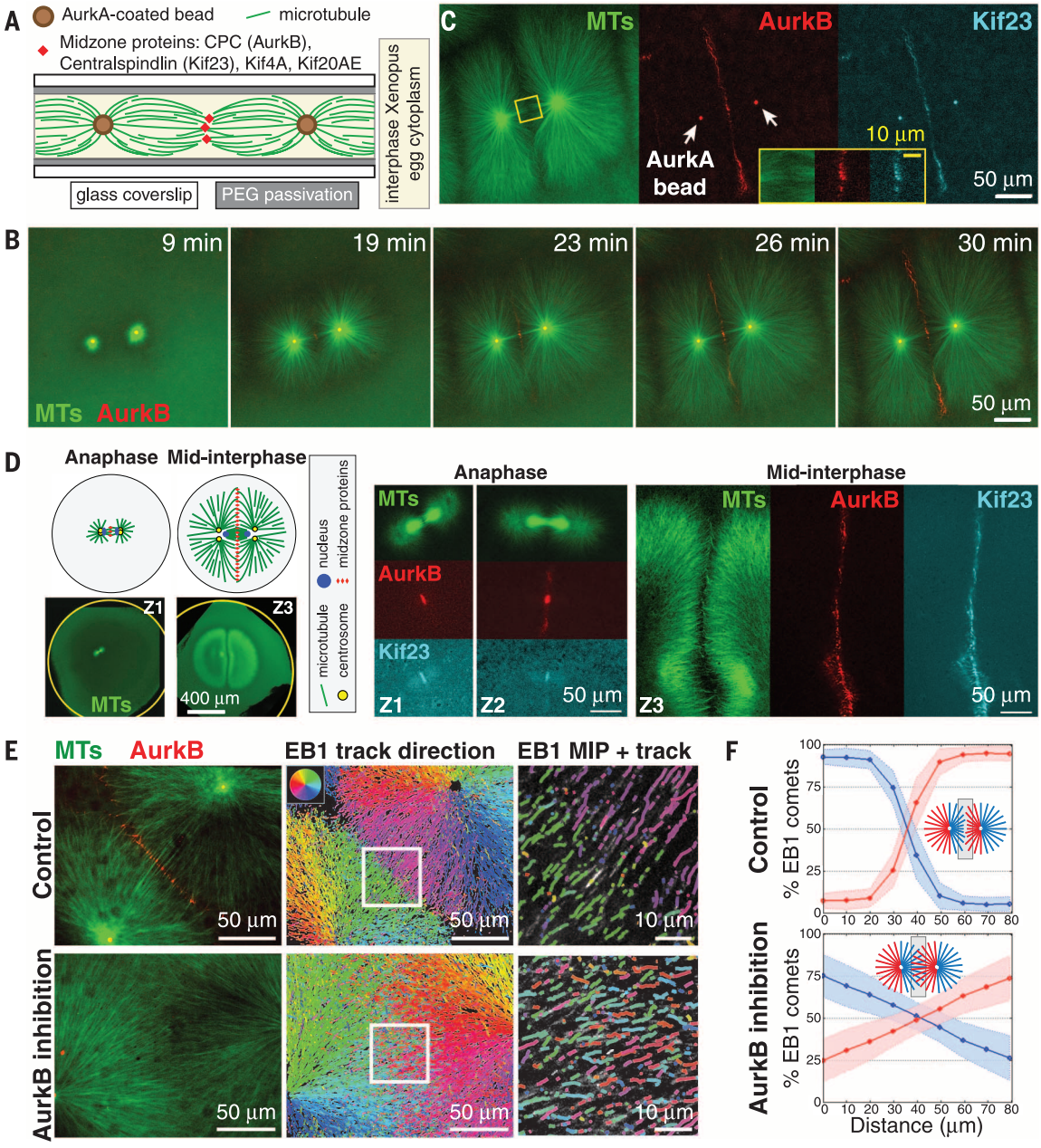

Fig. 1. Aster outgrowth and interaction in *Xenopus* egg cytoplasm. (**A**) Experimental setup. See (*5*) for methods and probes. (**B**) Widefield time-lapse images showing recruitment of AurkB (red) to an AAIZ. (**C**) AAIZ at 30 min (widefield) showing recruitment of AurkB (CPC subunit, red) and Kif23 (centralspindlin subunit, cyan). (**D**) Localization of microtubules (MTs) (green), AurkB (red), and Kif23 (cyan) in *Xenopus* zygotes fixed at consecutive stages of the first cell division (stages Z1 to Z3) imaged by laser scanning confocal microscopy (*5*). (**E**) Quantification of microtubule orientation using EB1 tracking. (Left) Spinning disc confocal images of control (top) and AurkB-inhibited (bottom) AAIZs. (Middle) Map of EB1-GFP trajectories over 2 min. (Right) ×4 zoom-up of square in middle panel with maximum intensity projection (MIP) of EB1 tracks over 15 s. (**F**) Spatial distribution of EB1 tracks at AAIZs classified by direction (shading indicates standard deviations determined from $n \geq 5$ zones). (See figs. S2 and S3 and (*5*) for data analysis.)

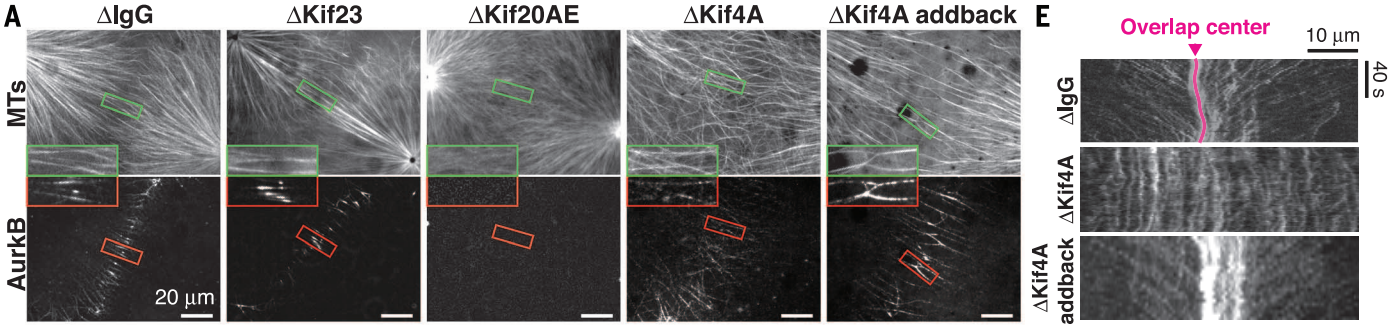

B

Kinesin candidate	Alternate names	Perturbation	CPC recruited	CPC focused
Control	NA	NA	+	+
Kif10	CenpE	inh	+	+
Kif11	Eg5	inh	+	+
Kif20A	Mklp2/rabkinesin-6	dep	+	+
Kif23	Mklp1/CHO1	dep	+	+
Kif4A	chromokinesin	dep	+	-
Kif20AE	NA	dep	-	-

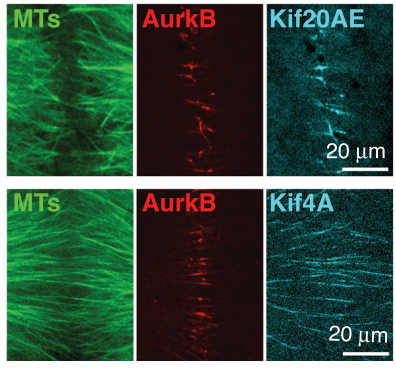

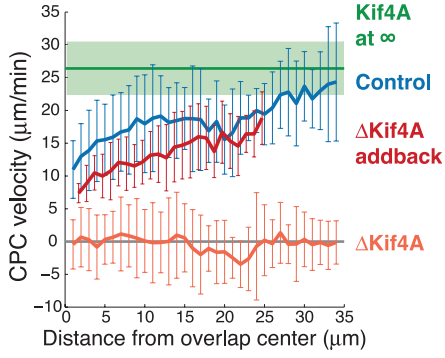

Fig. 2. Kinesin-dependent recruitment and motility of the CPC. (**A**) Representative spinning disc confocal images of microtubules and AurkB at AAIZs after kinesin immunodepletions, as labeled above. (**B**) Summary of kinesin perturbations using drug inhibition (inh) or immunodepletion (dep) (*5*). (**C** and **D**) Localization of Kif20AE and Kif4A at AAIZs (*5*). (**E**) Kymographs of CPC dynamics on individual microtubule bundles in AAIZs. (**F**) CPC velocity as a function of distance from the center of the AAIZ [error bars are standard deviations determined from $n \geq 3$ microtubule bundles (*5*)].

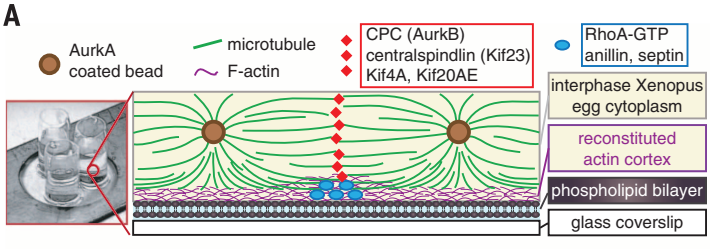

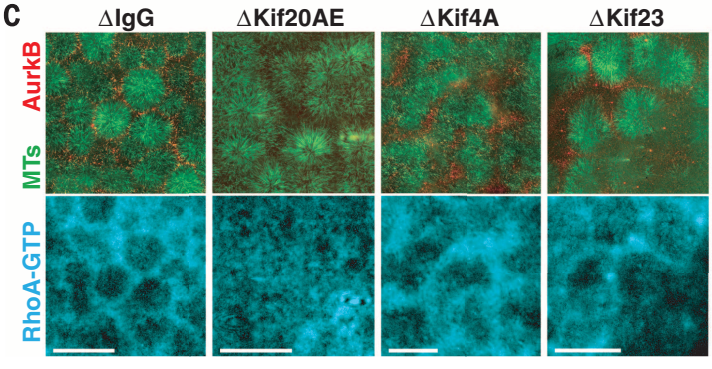

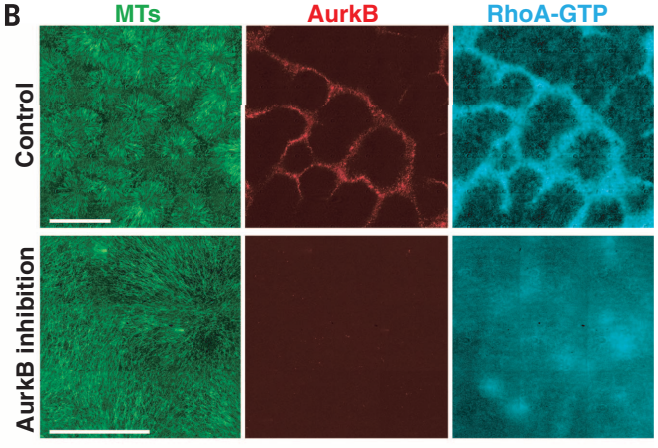

Fig. 3. Spatially localized recruitment of GTP-bound RhoA on model plasma membranes. (**A**) Drawing of experimental setup. See (*5*) for methods and probes. (**B** and **C**) Localization of a probe for RhoA-GTP (mCherry-rGBD; cyan) (*16*) and AurkB (red) at lipid bilayers proximal to AAIZs. TIRF images from 3 × 3 to 5 × 5 adjacent fields were corrected for uneven illumination and stitched (*5*). (B) Representative images of control and AurkB inhibition. (**C**) Representative images of kinesin immunodepletions, as labeled above. Scale bar, 200 μm.

using total internal reflection fluorescence (TIRF) microscopy (Fig. 3A). The small GTPase RhoA is thought to be the master organizer of the furrow (*16*). To localize active, GTP-bound RhoA we added an mCherry-tagged RhoA binding fragment of Rhotekin (mCherry-rGBD) (*16*). Using polyethylene glycol (PEG)–passivated coverslips, we saw no recruitment of RhoA-GTP. Using lipid bilayers, the RhoA-GTP reporter was enriched at the bilayer under AAIZs that recruited CPC and centralspindlin (Fig. 3B and fig. S12). Inhibition of AurkB or depletion of Kif20AE completely blocked AAIZ assembly and CPC localization as expected (*8*, *9*) and also blocked localized RhoA-GTP enrichment (Fig. 3, B and C). Kif4A depletion resulted in the broadening of both CPC and RhoA-GTP zones (Fig. 3C). Depletion of Kif23, a subunit of the centralspindlin complex, did not block AAIZ assembly or RhoA-GTP recruitment (Fig. 3C). Centralspindlin plays a central role in midzone assembly and signaling in many biological systems (*2*). Its dispensability in our system probably reflects functional redundancy among midzone factors and is consistent with its dispensability

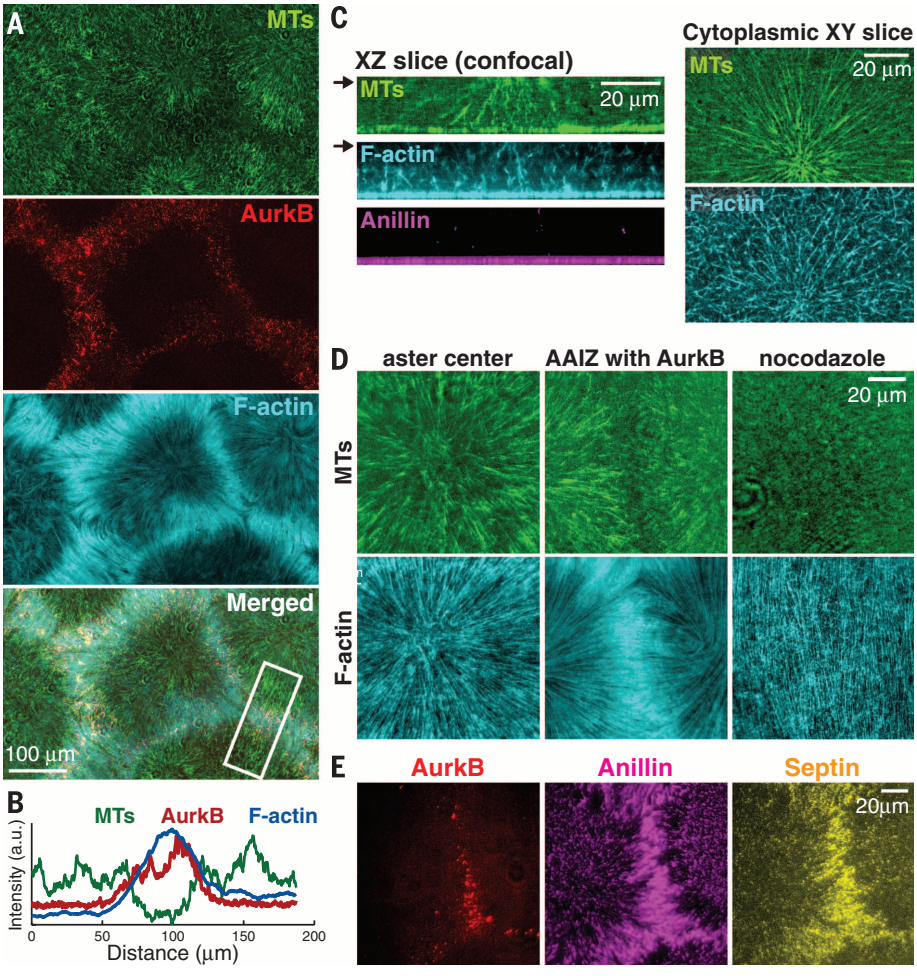

Fig. 4. Recruitment and organization of cortical cleavage furrow proteins. Experimental setup was as per Fig. 3A. (**A**) F-actin (TIRF image). Note the enrichment proximal to the CPC at AAIZs. (**B**) Intensity line scans across the AAIZ [boxed in (A)] show enrichment of AurkB and F-actin; a.u., arbitrary units. (**C**) XZ slices of three-dimensional reconstructions using spinning disc confocal microscopy, showing the organization of the microtubules, F-actin, and Anillin (left). XY slices of microtubules and F-actin at the plane marked by an arrow (right). (**D**) TIRF images of microtubules and F-actin at aster center (left) and an AAIZ (middle). The right shows a nocodazole-treated sample. (**E**) Anillin and septin on a bilayer (TIRF image) colocalize with the CPC at the AAIZ.

in *Xenopus* blastomere cytokinesis (*17*). We conclude that a CPC-positive AAIZ can locally activate RhoA in our system, although we cannot distinguish whether localized AurkB phosphorylation of cytokinetic factors or some specific organization of microtubules at the AAIZ is required for furrow signaling.

To probe cortical organization in our system, we visualized F-actin using Lifeact-GFP (Fig. 4) (*18*). F-actin was enriched at the lipid bilayer under AAIZs (Fig. 4, A and B). Above the cortical layer, F-actin organized into branched networks that showed only partial alignment with the microtubules (Fig. 4C). At the cortical layer, F-actin organized into long, uniformly spaced cables that aligned radially with microtubules (Fig. 4D, left and middle, and movie S9). The spacing between actin cables was 1.3 ± 0.5 µm (SD; n = 140), comparable to the spacing of actin-containing contractile bands on the cortex of live frog eggs (*19*). This organization was microtubule-dependent (Fig. 4D, right); we suspect it represents a configuration of actin bundles that normally precedes furrow ingression, because it has been noted in early anaphase in several systems (*5*). The furrow-selective actin bundling protein Anillin (*20*) colocalized with F-actin cables throughout the cortex and was enriched under AAIZs along with its binding partner septin complex (Fig. 4, C and E, and movie S10).

Summarizing, we have developed a cell-free system that recapitulates the hallmarks of spatially organized signaling characteristic of egg cytokinesis. Midzone proteins were recruited to the overlap zone between microtubule asters in egg extract, where they signaled to a nearby lipid bilayer to locally activate the RhoA pathway. Our system confirmed known mechanisms of spatially organized signaling (for example the AurkB activity requirement for cleavage furrow induction) and revealed new mechanistic aspects that were difficult to observe in living cells, notably transport of the CPC along microtubules toward the midzone in a process requiring two kinesins. Our data favor a model in which Kif4A is a transport motor for the CPC, and Kif20AE is required for it to bind microtubules, though not necessarily as a transporter. Future pure protein reconstitution experiments are required to conclusively determine the mechanism of CPC transport and the exact roles of these two kinesins.

Two factors facilitated imaging approaches in the cell-free system: the large spatial scale of the AAIZ (~20 µm) and its long time duration (>20 min). Both reflect the pre-cytokinesis organization of the large egg cell. In comparison, the microtubule overlap in somatic cell midzones is ~2 to 3 µm wide and lasts only ~3 min before being compressed by the furrow (*21*). Future studies will take advantage of these features and the experimental flexibility of an extract system to probe biophysical mechanisms involved in cytokinesis.

REFERENCES AND NOTES

1. R. Rappaport, *Cytokinesis in Animal Cells* (Cambridge Univ. Press, Cambridge, 1996).
2. M. Glotzer, *Science* **307**, 1735–1739 (2005).
3. C. M. Field, P. A. Nguyen, K. Ishihara, A. C. Groen, T. J. Mitchison, *Methods Enzymol.* **540**, 399–415 (2014).
4. M.-Y. Tsai, Y. Zheng, *Curr. Biol.* **15**, 2156–2163 (2005).
5. Supplementary materials are available on *Science* Online.
6. M. Wühr, E. S. Tan, S. K. Parker, H. W. Detrich 3rd, T. J. Mitchison, *Curr. Biol.* **20**, 2040–2045 (2010).
7. S. Petry, A. C. Groen, K. Ishihara, T. J. Mitchison, R. D. Vale, *Cell* **152**, 768–777 (2013).
8. H. Argiros, L. Henson, C. Holguin, V. Foe, C. B. Shuster, *Cytoskelet. Hoboken NJ* **69**, 840–853 (2012).
9. U. Gruneberg, R. Neef, R. Honda, E. A. Nigg, F. A. Barr, *J. Cell Biol.* **166**, 167–172 (2004).
10. R. A. Cross, A. McAinsh, *Nat. Rev. Mol. Cell Biol.* **15**, 257–271 (2014).
11. M. Wühr *et al.*, *Curr. Biol.* **24**, 1467–1475 (2014).
12. N. Ozlü *et al.*, *Mol. Cell. Proteomics* **9**, 336–350 (2010).
13. P. Bieling, I. A. Telley, T. Surrey, *Cell* **142**, 420–432 (2010).
14. T. J. Mitchison, P. Nguyen, M. Coughlin, A. C. Groen, *Mol. Biol. Cell* **24**, 1559–1573 (2013).
15. M. Loose, E. Fischer-Friedrich, J. Ries, K. Kruse, P. Schwille, *Science* **320**, 789–792 (2008).
16. W. M. Bement, H. A. Benink, G. von Dassow, *J. Cell Biol.* **170**, 91–101 (2005).
17. A. L. Miller, W. M. Bement, *Nat. Cell Biol.* **11**, 71–77 (2009).
18. J. Riedl *et al.*, *Nat. Methods* **5**, 605–607 (2008).
19. M. V. Danilchik, E. E. Brown, K. Riegert, *Development* **133**, 4517–4526 (2006).
20. A. F. Straight, C. M. Field, T. J. Mitchison, *Mol. Biol. Cell* **16**, 193–201 (2005).
21. D. N. Mastronarde, K. L. McDonald, R. Ding, J. R. McIntosh, *J. Cell Biol.* **123**, 1475–1489 (1993).

ACKNOWLEDGMENTS

We thank R. Ohi, D. Burgess, D. Miyamoto, and E. Tan for reagents; H. Basu for preliminary work; the Nikon Imaging Center at Harvard Medical School and Nikon at the Woods Hole Marine Biological Laboratory (MBL) for microscopy support; and the National Xenopus Resource at MBL for *Xenopus* animals and care. This work was supported by NIH grant GM39565 (T.J.M.); MBL fellowships from the Evans Foundation, MBL Associates, and the Colwin Fund (T.J.M. and C.M.F.); HFSP fellowship LT000466/2012-L (M.L.); and NIH grant GM103785 (M.W.).

SUPPLEMENTARY MATERIALS

www.sciencemag.org/content/346/6206/244/suppl/DC1
Materials and Methods
Supplementary Text
Figs. S1 to S13
Tables S1 to S2
References (*22–29*)
Movies S1 to S10

30 May 2014; accepted 12 September 2014
10.1126/science.1256773